

NOTES AND CORRESPONDENCE

Typhoon Rammasun-Induced Near-Inertial Oscillations Observed in the Tropical Northwestern Pacific Ocean

Eung Kim, Dongchull Jeon *, Chan Joo Jang , and Jae-Hun Park

Ocean Circulation and Climate Research Division, Korea Institute of Ocean Science and Technology, Ansan, Korea

Received 6 September 2012, accepted 28 March 2013

ABSTRACT

Wind-induced near-inertial oscillations (NIOs) have been known to propagate their energy downward and equatorward, yet few observations have confirmed this in tropical regions. Using measurements from a moored ADCP in the tropical northwestern Pacific, we report an energetic NIO event associated with Typhoon Rammasun in May 2008, when an anti-cyclonic warm eddy existed around the mooring site. Our analyses reveal that the anti-cyclonic eddy traps the NIO energy at two layers around 120 and 210 m where the buoyancy frequency show high values. The NIO energy continuously decays at layers below its maximum at 210 m, and disappears at depths below the thermocline. During their propagation from 137 to 649 stretched-meter depths (equivalent to 100 - 430 m), NIOs shift their frequencies from $0.92f$ to $1.05f$ probably due to the effective f , which changes its magnitude from smaller to larger than local inertial frequency f in the anti-cyclonic eddy. In addition, their vertical energy propagation becomes faster from 0.17 to 0.64 mm s⁻¹. Decomposition of downward and upward NIO energy propagation shows that the typhoon-induced NIOs remain 29% of their energy in the upper layer, and transfer 71% to the subsurface layers. Our results suggest that typhoon-induced NIOs interacting with meso-scale eddies can play an important role in providing the energy source available for ocean mixing in the tropical regions.

Key words: Near-inertial oscillation, Typhoon Rammasun, Anti-cyclonic eddy, Vertical variation of NIO frequency, ADCP currents

Citation: Kim, E., D. Jeon, C. J. Jang , and J.-H. Park, 2013: Typhoon Rammasun-induced near-inertial oscillations observed in the tropical Northwestern Pacific Ocean. *Terr. Atmos. Ocean. Sci.*, 24, 761-772, doi: 10.3319/TAO.2013.03.28.01(Oc)

1. INTRODUCTION

Wind-induced near-inertial oscillations (NIOs) are ubiquitous in the open ocean. After being generated NIOs generally propagate equatorward, yet they propagate northward up to a 'turning latitude' and then turn equatorward due to the β -effect (Anderson and Gill 1979; Alford 2003). They also propagate downward with different characteristics depending on wind strength, thickness of the mixed layer, and buoyancy frequency (Gerkema and Shrira 2005; Park et al. 2009; Byun et al. 2010). NIO breaking plays an important role in undermining the thermocline strength contributing to vertical mixing (Srifer and Huber 2007; Jaimes and Shay 2010). Background current fields can modify NIO propagation. For example, anti-cyclonic eddies create waveguides

trapping and amplifying NIOs (Kunze 1985; Lee and Niller 1998; Park and Watts 2005). In addition, large-scale currents, such as the Gulf Stream and the Kuroshio, advect and disperse NIOs (Zhai et al. 2004; Park et al. 2010).

Previous studies, including those mentioned above, are mostly about measurements of NIOs near the continental shelf or at mid and high latitudes in the open ocean (e.g., Alford 2003; Alford and Whitmont 2007), probably due to rare opportunities to observe them at low latitudes. In this study, we report an energetic typhoon-induced NIO event in the tropical northwestern Pacific, based on data from a moored upward-looking 75-kHz acoustic Doppler current profiler (ADCP). In addition, we also discuss NIO energy and period, both of which vary during vertical propagation, as well as the impact of the background currents on the dispersion of NIOs around the mooring site.

* Corresponding author
E-mail: dcjeon@kiost.ac

2. DATA AND METHODS

A subsurface buoy system had been moored at a site (15.8°N, 134.6°E) with 3080 m of the water depth in the tropical northwestern Pacific from October 8, 2007 to June 16, 2008; the mooring site was located near the core of the most frequent typhoon passages (Fig. 1a). The observation device consisted of a 75-kHz upward-looking ADCP at 525 m. The ADCP was set to have a bin thickness of 16 m, and hourly currents were obtained after the ensemble averaging 10 pings per hour. Due to a tilting of the mooring line, the bin depths of ADCP measurements varied over time. Thus, the current measurements were interpolated into 10 m intervals between 50 and 500 m. Then, to focus on NIOs, the data were band-pass filtered with cut-off frequencies between $0.73f$ and $1.22f$, where f is the local inertial frequency ($= 3.97 \times 10^{-5} \text{ s}^{-1}$).

Buoyancy frequencies were calculated using *in-situ* temperature-salinity profiles from an ARGO profiling float (S/N 2900628) which was located within 45 km of the mooring site during the passage of Typhoon Rammasun. Buoyancy frequency can change the amplitude and vertical wavelength of NIOs as it propagates vertically (Leaman and Sanford 1975). Thus, the filtered velocity profiles to delineate NIOs are normalized in terms of WKB (Wentzel-Kramers-Brillouin) approximation scheme (Leaman and Sanford 1975). The normalized velocity (u_n) is given by

$$u_n(z) = \frac{u(z)}{\sqrt{[\bar{N}(z)/N_0]}} \quad (1)$$

where $u(z)$ is the raw velocity component for a given profile at depth z , \bar{N} is the time-mean buoyancy frequency cal-

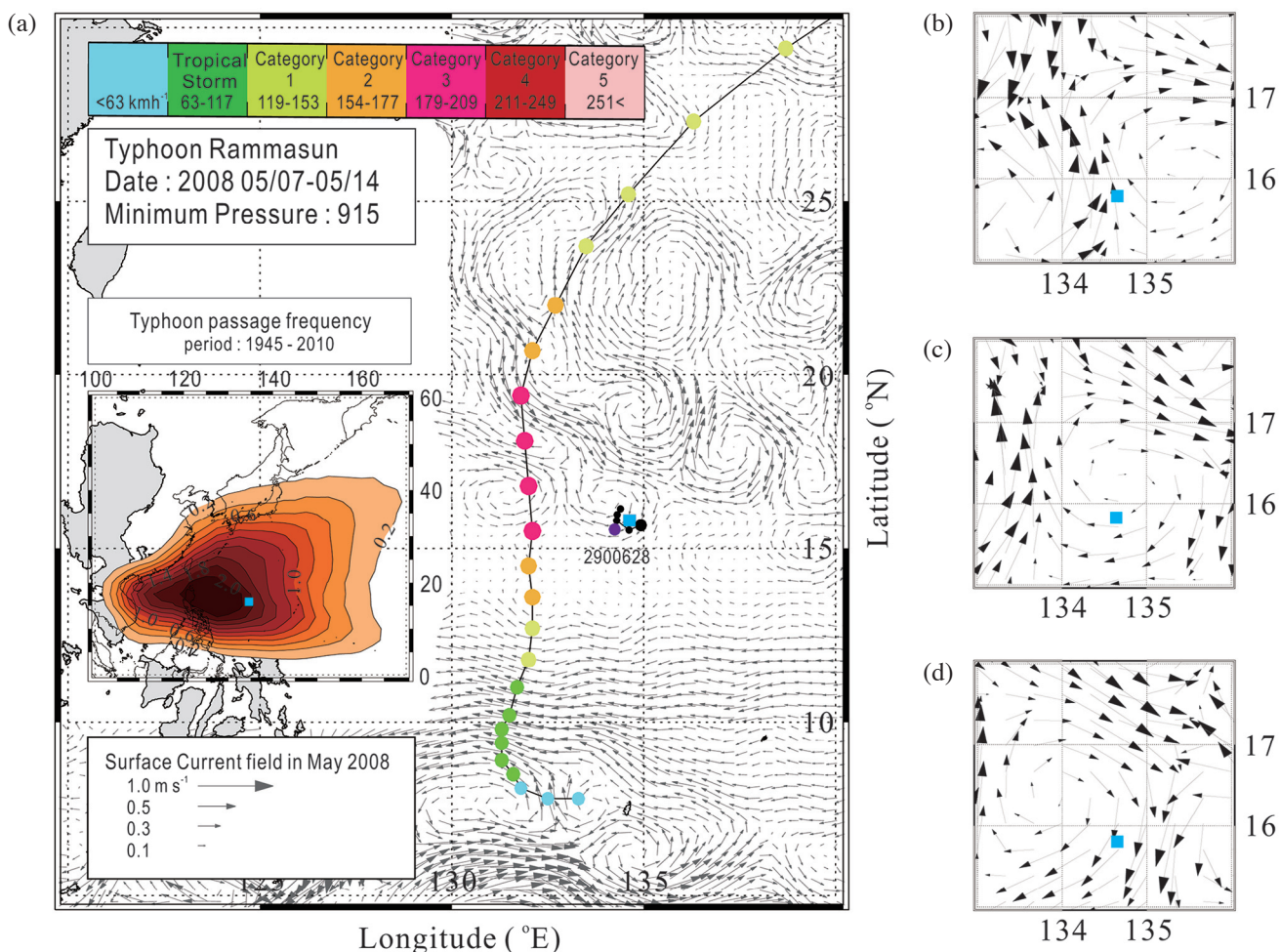


Fig. 1. (a) Mooring site (■) in the tropical northwestern Pacific Ocean and the track of Typhoon Rammasun which occurred in May 2008. Background arrows show the monthly mean surface current field calculated from AVISO data in May 2008. Filled color circles show the central positions of Rammasun every 6 hours from the Joint Typhoon Warning Center track data, and color represents typhoon category. Small box shows Typhoon passage frequency per year in each $2.5^\circ \times 2.5^\circ$ grid area for the period 1945 ~ 2010. Black circles (●) near the mooring site indicate the locations of an ARGO profiling float (S/N 29000628) and the violet circle (●) indicates its last location. Surface current fields calculated from AVISO data on (b) May 7, 2008, (c) May 14, 2008, and (d) May 21, 2008.

culated from ARGO float, and N_0 is a reference buoyancy frequency equal to 3.85 cph (mean buoyancy frequency between 15 and 995 m depths). The vertical coordinate is stretched by the differential law

$$d_{z_n} = \frac{\bar{N}(z)}{N_0} \quad (2)$$

where z and z_n are the physical and stretched coordinates, respectively. Table 1 compares depths between the two coordinates.

In order to estimate the vertical propagation speed of NIOs triggered by a typhoon, average NIO kinetic energy density with a local inertial period (= 43.9 hours) is calculated as follows (Zheng et al. 2006):

$$\bar{E}_k = \frac{\rho}{4} \left[\frac{\sum_{i=1}^l (u^2, v^2)_{k+i}}{2l+1} \right] \quad (3)$$

where ρ is seawater density calculated from the ARGO float data during the typhoon passage, k and i are time series number of data point and sequential number in a window, respectively, and the duration ($2l$) used to obtain an averaged value is similar to the local inertial period, implying that l equals to 22.

Effective Coriolis frequency, $f_{\text{eff}} = f + \zeta/2$, where f and ζ are local inertial frequency and relative vorticity (Kunze and Sanford 1984) respectively, were calculated using velocity fields from the data-assimilated HYbrid Coordinate Ocean Model (HYCOM) outputs with the spatial resolution of $1/12^\circ\text{E} \times 1/12^\circ\text{N}$ and the temporal resolution of 1 day (Wallcraft et al. 2009). Details of the HYCOM simulations are found at their website (<http://www.hycom.com>). In order to obtain the relative vorticity around the mooring site, zonal gradient of north-southward current v ($= dv/dx$) and meridional gradient of east-westward current u ($= du/dy$) are calculated.

QuikSCAT daily-mean winds, produced by the French Research Institute for Exploration of the Sea (IFREMER) near the mooring site before and after passage of the typhoon, were analyzed to investigate the relationship between the local winds and the occurrence of NIOs.

3. TYPHOON RAMMASUN AND THE OCEANOGRAPHIC SETTING

Typhoon Rammasun originated on May 6, 2008 near 7.2°N , 134.2°E and finished its lifetime as a tropical storm on May 13 near 33.4°N , 146.8°E (<http://www.usno.navy.mil/JTWC>). It grew to be a category 3 and 4 typhoon during May 10 - 11, 2008, and then moved northward along 132°E (Fig. 1a). At the closest approach on May 10, 2008, it was 270 km to the west of the mooring site with a minimum sea

level pressure of 929 hPa and a maximum sustained wind speed of 33 m s^{-1} . The radius of a maximum sustained wind speed (R_{max}) was about 70 km, and the radius of winds with 17.5 m s^{-1} or greater was between 268 and 287 km. Time series of QuikSCAT daily-mean winds interpolated at the mooring site show easterly winds of about 5 m s^{-1} or less before the passage of typhoon Rammasun (Figs. 1a and 3b). Strong southeasterlies with speeds of $12 - 16 \text{ m s}^{-1}$ occurred during the passage of typhoon (May 9 - 11); weaker southeasterlies to southwesterlies with speeds of about 6 m s^{-1} or less continued for a week after the passage.

The upper bound of the thermocline measured by the ARGO float (Fig. 2a) deepened from 80 to 120 m during May 5 - 25, and the thicknesses of the mixed layer and the thermocline are 120 and 340 m, respectively (Fig. 2b). Deepening of the thermocline is mainly due to the passage of an anti-cyclonic eddy as shown in the time series of surface current fields from AVISO data (Figs. 1b - d). Deepening of the mixed layer on May 15 seems to be a signature of the typhoon, but the 10-day interval of ARGO profiler is not enough to detect the typhoon response in detail. The mean buoyancy frequency profile estimated using two hydrocasts on May 15 and 25 after the passage of typhoon reveals three peaks near 135, 210, and 390 m, and two minimal values near 174 and 330 m (Fig. 2b). At the mooring site, the spectral frequency of the vertically-averaged zonal currents between 50- and 100-m depths is $3.73 \times 10^{-5} \text{ s}^{-1}$ ($= 0.94f$), which is smaller than the local inertial frequency (Fig. 3a) although there is a limitation that the frequency resolution in the spectral analysis cannot resolve the exact frequency of NIO. The time-varying spectra of NIOs estimated by the wavelet on the vertically-averaged zonal component of currents between 50 and 100 m begin to appear after a strong wind event due to Typhoon Rammasun on May 9, and then show the peak on May 12 (Fig. 3b).

NIOs occurred after May 7, 2008, when the tropical depression grew to the tropical storm (Figs. 4, 5a, and 5b), and an anti-cyclonic eddy (Figs. 1b to d) existed in May 2008 when Typhoon Rammasun passed over the mooring site. To understand the relationship between the eddy and typhoon, ADCP data are traced since May 1, 2008, for oceanic conditions before the passage of the typhoon (Fig. 5). May 1 is set -4 in time/IP where time is in Julian day with the basic date of May 7, 18:00 being day '0'; IP is the local inertial period (= 43.9 hours). The progressive vector diagram (Fig. 4) at all depths from May 1 to 29 displays a change in flow direction from a northwestward to southwestward which seems to be caused by the anti-cyclonic eddy. The directional change of the major currents is related to the westward propagation of the anti-cyclonic eddy at the mooring site (Figs. 1b to d); it is northwestward when the center of anti-cyclonic eddy is located to the northeast of the mooring site (Fig. 1b), and southwestward when its center is to the northwest (Fig. 1d), respectively. In addition to the low-frequency motion, the

diagram also shows high-frequency motions related with NIOs. In the progressive vector diagram (Fig. 4), T (= May 10, 2008) indicates the point when the typhoon approaches the closest to the mooring site, E (= May 16, 2008) indicates the changing point in current direction from northwest to southwest by an anti-cyclonic eddy, and I_s and I_e indicate the start and end-points of a few cycles in near-inertial motion used to calculate the frequency. I_s and I_e are technically defined as the turning points in meridional direction to span complete 3 or 4 inertial cycles, which are arbitrarily chosen from a progressive vector track with an hourly interval data. The mean frequency of the near-inertial motion at each depth is averaged for the selected 3 or 4 cycles (Table 2), which increases from $3.85 \times 10^{-5} \text{ s}^{-1}$ at 100 m to $4.36 \times 10^{-5} \text{ s}^{-1}$ at 350 m. The ratio of the mean frequency to the local inertial frequency ($= 3.97 \times 10^{-5} \text{ s}^{-1}$) also increases from 0.97 to 1.1 with increasing depth.

The zonal currents, low-pass filtered with the cut-off frequency at $0.73f$ ($= 60.1$ hours), are predominantly westward (Fig. 5c). The meridional currents (Fig. 5d) are northward before May 16 and changes southward after May 16. These results indicate that typhoon-induced NIOs occurred during the period when the mooring site was located near the southern boundary of the anti-cyclonic eddy. Surface geostrophic currents estimated from altimeter data show that an anti-cyclonic eddy with a diameter exceeding 200 km around the mooring site propagates westward in May 2008 (Figs. 1b to d).

Horizontal components of the NIOs (Figs. 5e and f) show propagations of downward energy and upward phase at depths from 59 to 725 stretched meter (sm) during May 10 - 30 after the passage of Typhoon Rammason. The vertical distribution of NIOs is classified into three layers according to the maxima and minima of the buoyancy frequency.

Table 1. Comparison of real (z) and stretched (z_n) depth levels at the mooring site (sm: stretched meter).

z (m)	50.0	90.0	120.0	170.0	210.0	230.0	270.0	350.0	430.0	500.0
z_n (sm)	59.7	118.2	179.2	281.3	347.6	382.9	443.3	545.3	649.7	725.5

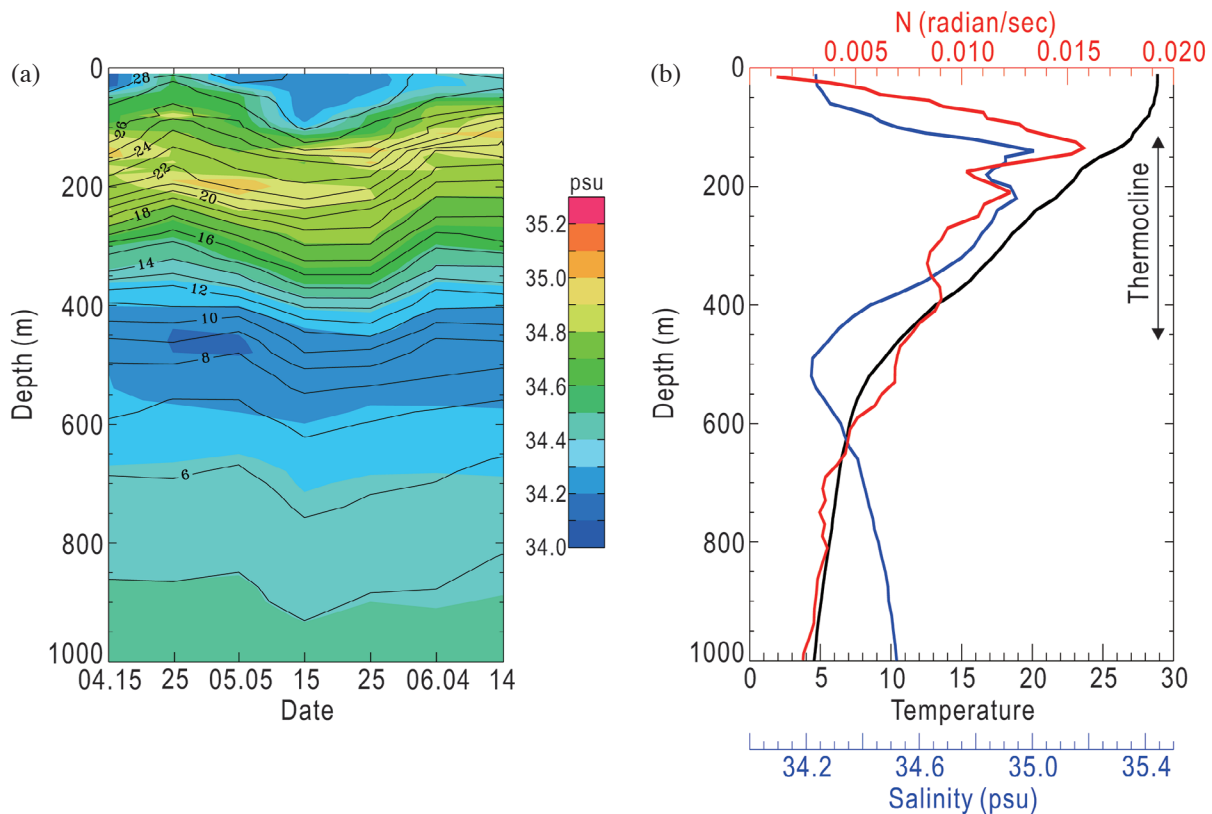


Fig. 2. (a) Time series of temperature (line contours) and salinity (colored contours) profiles observed from the ARGO float from April 15 to June 14, 2008. Dates of x-axis are observation times cast by ARGO float with 10-day interval. (b) Mean vertical profiles of temperature (black), salinity (blue), and buoyancy frequency (red) estimated using two hydrocasts on May 15 and May 25, 2008 after the passage of Typhoon Rammason.

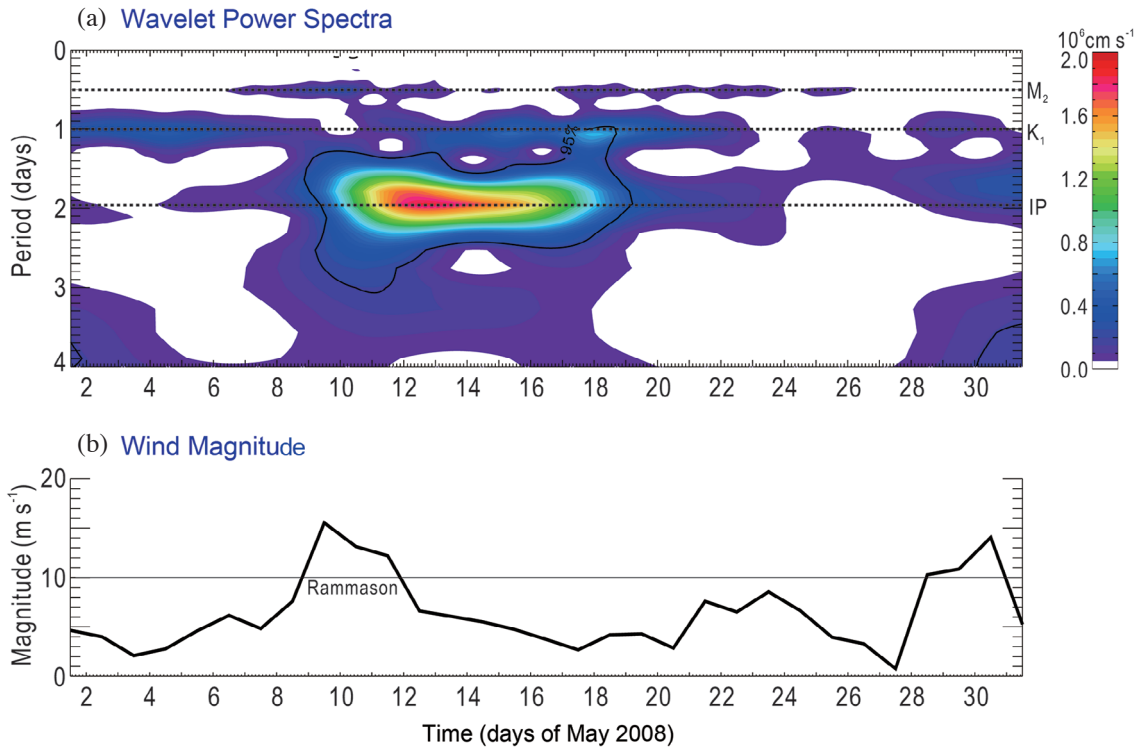


Fig. 3. (a) Wavelet power spectra calculated from the vertically- averaged zonal component of currents between 50 and 100 m during the whole observational period. Spectral values lower than the 95% significance level are omitted. Dotted lines indicate M_2 and K_1 tidal periods, and local inertial period (IP). (b) Time-series of QuikSCAT daily-mean winds nearest the mooring site during the observational period.

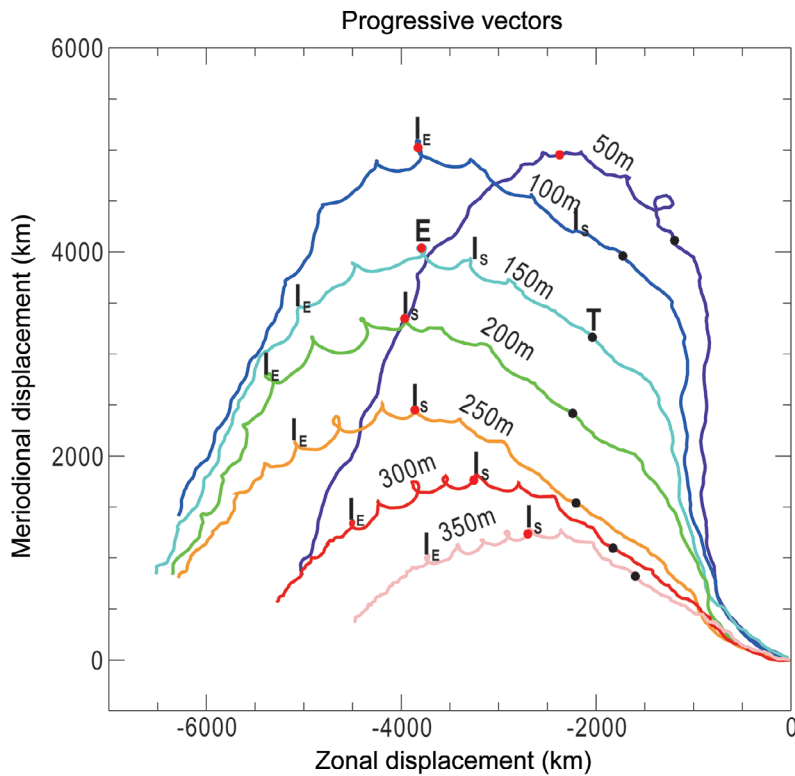


Fig. 4. Progressive vector diagram at each depth, calculated using current measurements between May 1 and May 29, 2008. T (●) indicates when the typhoon approaches closest to the mooring site, E (●) indicates the change of current direction by an anti-cyclonic eddy, I_s and I_e indicate the start and end-points of arbitrarily-chosen (3 or 4) cycles of near-inertial motion used to calculate the periods.

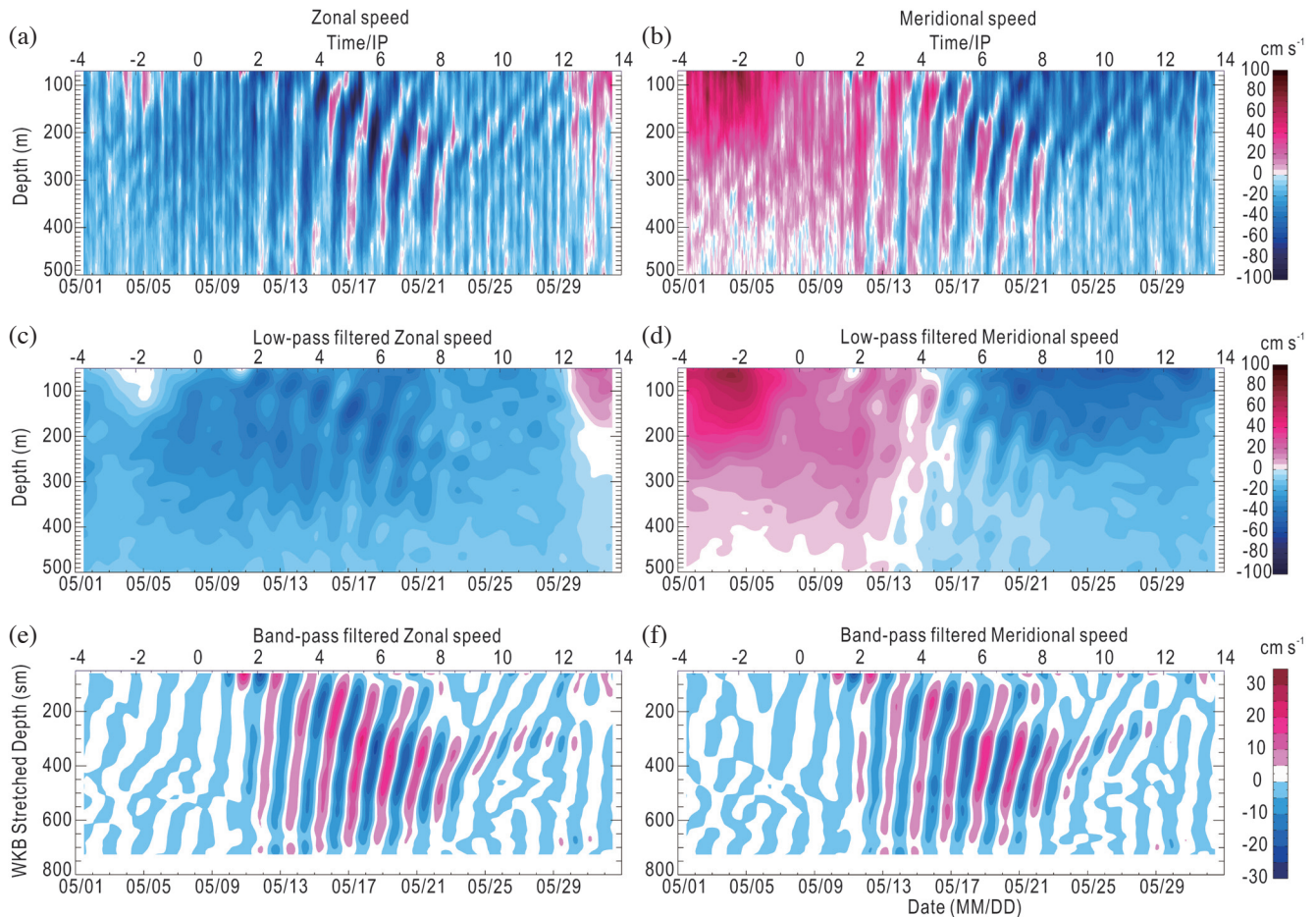


Fig. 5. Panels showing zonal and meridional velocity components: zonal (a) and meridional (b) velocities of raw ocean currents, zonal (c) and meridional (d) velocities of low-pass filtered currents ($0.73f$ cut-off frequency), and zonal (e) and meridional (f) velocities of band-pass currents ($0.73f$ to $1.22f$) normalized by the WKB. Vertical coordinate is stretched by the WKB method. The labels on upper x-axis are the dates calculated from time/IP, where IP ($= 43.9$ hours) is the local inertial period at the mooring site, and time is in Julian day: '0' represents the day of May 7, 2008 (at 18:00) when it grew from tropical depression to tropical storm.

Table 2. Mean periods of near-inertial motions by 50 m interval between 100 and 350 m calculated from the current measurements. Ratio is calculated by dividing the mean frequency by the local inertial frequency ($= 3.97 \times 10^{-5} \text{ s}^{-1}$).

Depth (m)	Time at start point (I_s) in [dd/hh]	Time at end point (I_e) in [dd/hh]	Cycles	Mean frequency ($\times 10^{-5} \text{ s}^{-1}$)	Ratio
100	11/07	16/21	3	3.85	0.97
150	14/17	20/05	3	3.99	1.01
200	16/08	21/17	3	4.06	1.02
250	16/08	21/11	3	4.27	1.07
300	16/05	22/22	4	4.33	1.09
350	16/02	22/17	4	4.39	1.10

NIOs appear at the layer around 59 m during the early stage of the typhoon, and gradually disperse into the eddy core over time. At depths around 383 m ($= 230$ m) NIOs persist for the longest duration until May 31.

Table 3 lists conventional non-dimensional storm and air-sea parameters used in this study. These parameters are

estimated from the scale analyses proposed by Price (1983) and Price et al. (1994). Wind-driven horizontal and vertical velocities in mixed layer are 0.27 m s^{-1} and 0.47 mm s^{-1} , respectively. Burger numbers on mixed-layer and thermocline, the degree of pressure coupling between the mixed-layer current and the thermocline current (Price et al. 1994),

Table 3. Air/sea parameters and scaling on Typhoon Rammasun.

Parameter	Value
<i>Independent variable scales</i>	
Density of air	$\rho_a = 1.26 \text{ kg m}^{-3}$
Maximum wind speed	$U_{10} = 33 \text{ m s}^{-1}$
Radius to maximum wind stress	$R = 70 \text{ km}$
Storm translation speed	$U_H = 7.5 \text{ m s}^{-1}$
Wind stress	$\tau = \rho_a (0.49 + 0.065 U_{10}) \times 10^{-3} U_{10}^2 = 3.62 \text{ Pa}$
Mixed-layer thickness	$h_1 = 120 \text{ m}$
Thermocline scale thickness	$b = 340 \text{ m}$
Bottom depth	$D = 3080 \text{ m}$
Reduced gravity	$g' = 0.02 \text{ m s}^{-2}$
Mean seawater density across thermocline	$\rho_0 = 1024.8 \text{ kg m}^{-3}$
Density change across thermocline	$\Delta\rho = 4.18 \text{ kg m}^{-3}$
Coriolis frequency at 15.8°N	$f = 3.97 \times 10^{-5} \text{ s}^{-1}$
Local inertial period at 15.8°N	$\text{IP} = 2\pi/f = 43.9 \text{ hours}$
Reference buoyancy frequency	$N_0 = 3.85 \text{ cph}$
Vertical wave length	$\lambda_m = 115 \text{ m}$
Horizontal wave length	$\lambda_k = 4R = 280 \text{ km}$
Mean zonal current speed	$u = -0.29 \text{ m s}^{-1}$
Meridional mean current speed	$v = -0.21 \text{ m s}^{-1}$
<i>Dependent variable scales</i>	
Wind-driven horizontal velocity	$\tilde{U} = \tau R / \rho_0 h_1 U_H = 0.27 \text{ m s}^{-1}$
Wind-driven vertical velocity	$\tilde{U} h_1 / R = \tau / \rho_0 U_H = 4.7 \times 10^{-4} \text{ m s}^{-1}$
Horizontal particle displacement	$\tilde{U} / f = \tau R / \rho_0 f h_1 U_H = 6.9 \text{ km}$
Energy	$\tilde{U}^2 h_1 = \tau^2 R^2 / \rho_0^2 h_1 U_H^2 = 9.1 \text{ m}^2 \text{ s}^{-2}$
Isopycnal displacement	$\tilde{\eta} = \tau / \rho_0 f U_H = 11.9 \text{ m}$
Pressure	$\tilde{\eta} g' = g' \tau / \rho_0 f U_H = 0.24 \text{ m}^2 \text{ s}^{-2}$
Geostrophic velocity	$\tilde{\eta} g' / f R = g' \tau / \rho_0 f^2 U_H R = 0.085 \text{ m s}^{-1}$
<i>Non-dimensional parameters</i>	
Nondimensional storm speed	$S = U_H / 2Rf = 1.35$
Mixed-layer Burger number	$M = g' h_1 / 4f^2 R^2 (1 + 1/S^2) = 0.12$
Thermocline Burger number	$T = Mb / h_1 = 0.34$
Air/sea aspect ratio	$C = R / h_1 = 583$
Rossby number	$Q = 3\tau / (\rho_0 h_1 U_H f) = 0.3$
Vertical aspect ratio	$A = h_1 / D = 0.04$

are much smaller than one such as 0.12 and 0.34, respectively. These conditions indicate that the study region may be influenced by large-scale atmospheric forcing (Dukhovskoy et al. 2009). The Rossby number is also small ($= 0.3$) in the region, implying that non-local and advective effects are less important during the forcing stages (Dickey et al. 1998).

4. OBSERVATION OF TYPHOON-INDUCED NIOS

The NIO motions are generally dominated by clock-

wise rotation in the northern hemisphere. To extract rotating energy components of the NIO, the rotary spectra on the WKB normalized velocity components are calculated between 2 IP (May 11, 10:00) and 7 IP (May 20, 14:00) in the time-domain. Clockwise and anti-clockwise energies in each WKB normalized depth layer are selected on spectrally resolved frequency, 0.545 day^{-1} (44-hour period), where it is similar to the f . Clockwise energy is greater in the order of 1 than anti-clockwise energy each layer (Fig. 6a). The rotary coefficients of horizontal direction of propagation are

over 0.7 in almost the whole layers except below 650 sm. The positive values mean clockwise rotating in the northern hemisphere. These results confirm that the energetic fluctuations are caused by the NIOs.

Time series of the kinetic energy (Fig. 6b) calculated using band-pass-filtered zonal currents from May 9 to 30 show three peaks: 11 J m^{-3} at 50 m on May 11, 07:00 when the typhoon developed its maximum strength, 17 J m^{-3} at 120 m on May 16, 06:00, and 18 J m^{-3} at 210 m on May 18, 13:00. Even on May 21, 01:00, 10 days after the passage of the typhoon, the kinetic energy is 4 J m^{-3} at 350 m, which is higher than the background energy level before the typhoon event. The peaks of the averaged NIO kinetic energies are observed above 400 m in depth and the vertical locations of peaks except at the surface are consistent with buoyancy frequency peaks (Fig. 2b). The NIO kinetic energy becomes a little below 400 m and appears to be trapped in the lower boundary of the anti-cyclonic eddy (Fig. 6b). A similar effect has been noted in the numerical experiment by Lee and Niller (1998), where the NIO energy is trapped in the core of anti-cyclonic eddy and reaches its maximum at a critical layer where the effect of relative vorticity diminished.

Dissipation rates (ε) of kinetic energy are estimated using ARGO float hydrocasts and ADCP data for quantifying the turbulence and mixing processes in an anti-cyclonic eddy from the equation by Lueck and Osborn (1986).

$$\varepsilon = \frac{15}{4} \rho \nu \left[\left(\frac{\partial u}{\partial z} \right)^2 + \left(\frac{\partial v}{\partial z} \right)^2 \right] \quad (4)$$

where ρ is seawater density, ν is kinematic viscosity, and the terms in the bracket are vertical current shears. Figure 7 shows the dissipation rates on May 5, 15, and 25, 2008, re-

spectively, the typhoon passed near the mooring site on 15. They are small through the entire layers on May 5, increase over $4 \times 10^{-4} \text{ W m}^{-3}$ in upper layers and $1 \times 10^{-4} \text{ W m}^{-3}$ between 240 and 280 m below thermostad of the anti-cyclonic eddy core on May 15 and are large over $3 \times 10^{-4} \text{ W m}^{-3}$ between 200 and 250 m on May 25. The vertical structure of dissipation rates in the anti-cyclonic eddy is influenced by the propagation of NIOs. The trapped energy of NIOs at 210 m decays downward probably owing to the dissipation induced by turbulence in the anti-cyclonic eddy. The NIO energy gradually vanishes between 200 and 250 m before May 30.

The NIO energy propagates into deeper layers faster with increasing depths (Fig. 6b): 0.17 mm s^{-1} from two kinetic energy peaks between 50 and 120 m, 0.44 mm s^{-1} between 120 and 210 m, and 0.64 mm s^{-1} between 210 and 350 m. The vertical propagation speed (0.44 mm s^{-1}) in the middle layer is consistent with the vertical group velocity (C_{gz}), 0.46 mm s^{-1} , calculated from theoretical analysis (Rossby and Sanford 1976) as follows:

$$C_{gz} = -2 \times f \times \alpha \times m^{-1} \quad (5)$$

where α is the departure from f , which is set 0.05 (-0.05) following Jaimes and Shay (2010) on downward (upward) energy from Fig. 8a. The vertical propagation speed is similar to the value from the scale analysis (Table 3).

In order to examine the frequencies of NIOs propagating vertically from the sea surface, power spectral analysis is applied on the WKB normalized raw zonal components (Fig. 8a). Maximum peak of power spectrum exists at 347 sm (210 m). As the NIO propagates into deeper layers, the fre-

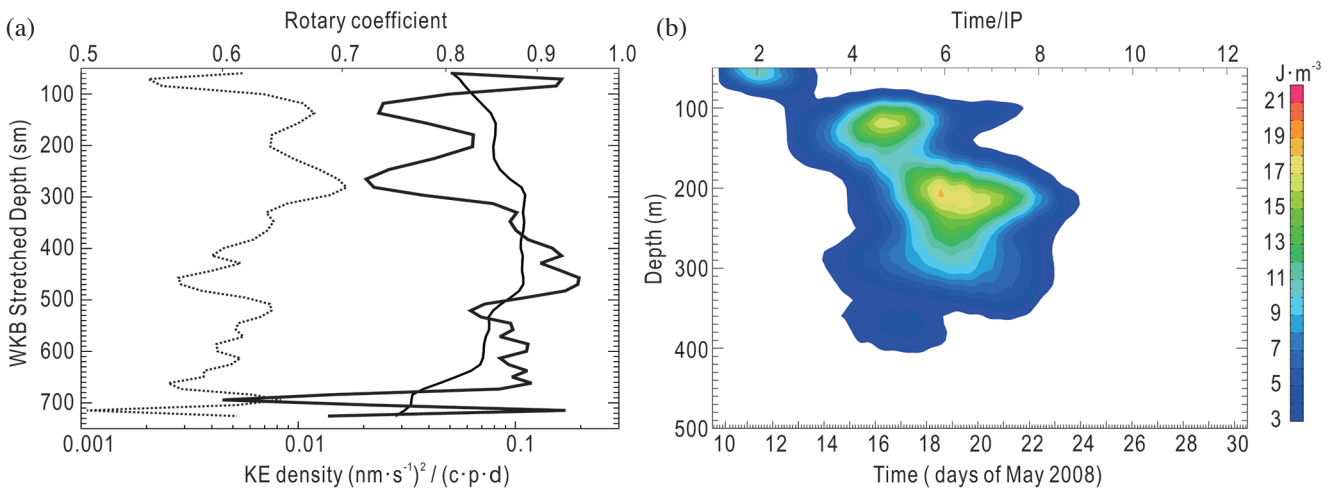


Fig. 6. (a) Energy distribution of local inertial frequency band (0.545 day^{-1}) resolved from horizontal rotary spectra each layer between 2 nd 7 IP (May 11, 10:00 ~ May 20, 14:00), dotted and thin curves are anti-clockwise and clockwise energies, respectively, and thick curve is rotary coefficient on local inertial frequency band. (b) Propagation of the average kinetic energy density of NIOs calculated by Zeng's (2006) equation.

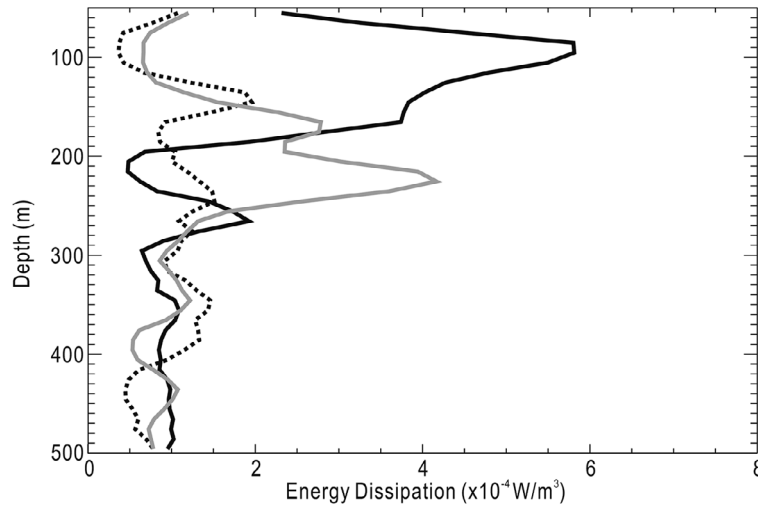


Fig. 7. Dissipation rate of kinetic energy estimated using ARGO float hydrocasts and ADCP data. The dotted, black, and gray curves show the energy dissipation profiles before (May 5, 2008), passing (May 15, 2008), and after (May 15, 2008) Typhoon Rammasun, respectively.

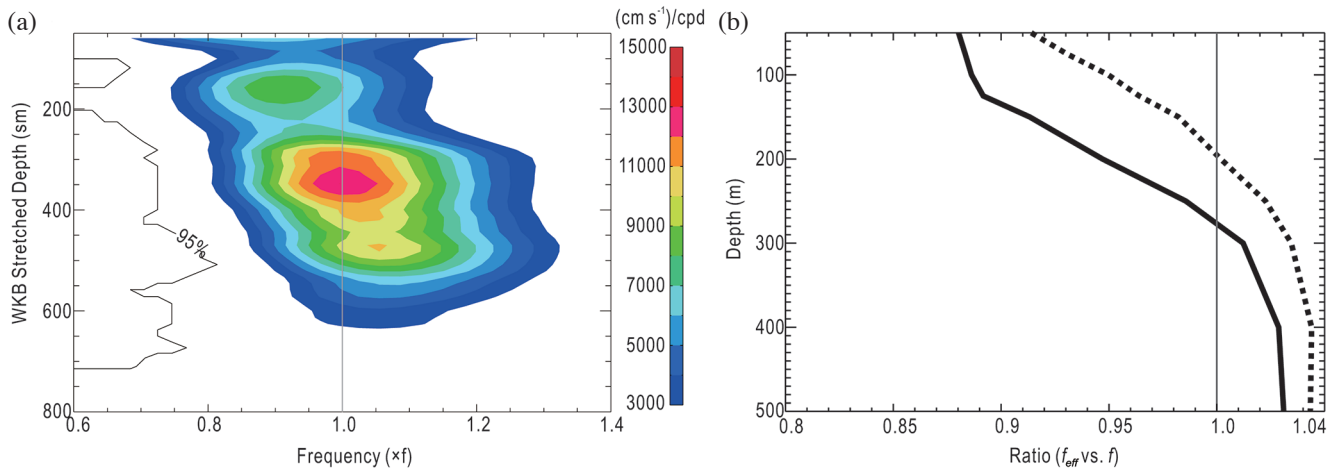


Fig. 8. (a) Change of NIO frequency (in units of the local inertial frequency) estimated from the wavelet spectrum with the WKB normalized zonal speeds. Thick curves denote 95% significance. (b) Ratios of the effective Coriolis frequency to the local Coriolis frequency, dotted and thick curves show before and after Typhoon Rammasun, respectively, and gray lines of (a) and (b) show the local Coriolis frequency as the ratio '1'.

quency at the peak of spectral density becomes higher such that it is $0.73f$ at depths from 84 to 118 m, $0.92f$ from 137 to 202 m, $1.0f$ from 281 to 365 m, and $1.05f$ from 443 to 649 m, respectively. A similar change of NIO frequency was found by Jaimes and Shay (2010): they show that the frequencies of Katrina-induced NIOs increased from $0.95f$ at the sea surface to $1.05f$ at depths below 300 m ($f = 6.85 \times 10^{-5} \text{ s}^{-1}$ at 27.998°N).

NIO frequencies estimated from the observed ADCP currents are affected by the change of f_{eff} ($= f + \zeta/2$) with depth. To understand the effect of f_{eff} , the data-assimilated HYCOM outputs (not normalized by WKB scheme) are used to calculate ζ . The ζ values change from negative in the upper layers (< 280 m) to positive in the lower layers (> 280 m). The ratio of f_{eff} to f gradually increases with in-

creasing depth as shown in Fig. 8b. Difference of the ratio between 100 and 400 m becomes larger after Rammasun than before. The ratio changes 0.96 to 0.89 at 125 m, and changes 1.04 to 1.03 at 400 m after the typhoon. The f_{eff} is smaller than f in the upper layers both before and after the typhoon with increasing amplitudes after the typhoon. Depth of ratio '1' deepens from 200 to 280 m after the typhoon. The increase of f_{eff} with depth is caused by the decrease of ζ amplitude because the anti-cyclonic eddy becomes weak with depth.

Vertical energy fluxes are calculated with the procedures of Leaman and Sanford (1975) and Jaimes and Shay (2010) on the WKB normalized band-pass filtered components between 3.5 IP (May 14, 03:00) and 5.5 IP (May 17, 18:00), following

$$E_{flux}(m) = E(m) \times C_{gz}(m) \quad (6)$$

where $E(m)$ is the energies of vertical rotary spectrum of m -th wavenumber. Downward (upward) energy fluxes are calculated from clockwise (anti-clockwise) energy in vertical rotary spectrum.

The kinetic energy densities of the vertical rotary spectrum are dominant in clockwise energies more than anti-clockwise energies, and the ratios of clockwise to anti-clockwise energies range from 1.8 to 2.8 between vertical wavelengths 112 and 337 sm (Fig. 9). Downward and upward energies integrated over the vertical wavelength are $13.7 \times 10^{-2} \text{ W m}^{-2}$ and $5.6 \times 10^{-2} \text{ W m}^{-2}$, respectively, on the mean seawater density in thermocline layer (1024.3 kg m^{-3}) estimated from ARGO data. Percentage of downward clockwise energy out of the total energy fluxes ($19.3 \times 10^{-2} \text{ W m}^{-2}$) is 71% and percentage of upward anti-clockwise energy is 29%, and the ratio of clockwise to anti-clockwise energies on total energies is 2.4. The result in anti-cyclonic eddy is similar to the vertical energy flux by tropical cyclones Katrina and Rita in Loop current (Jaimes and Shay 2010). This result suggests that 71% of Rammasun-induced near inertial energy propagates downward to be trapped in the core of eddy, and 29% of it may provide an energy source contributing to vertical mixing in the upper layer.

5. CONCLUSIONS

This study presents an energetic NIO event in the tropical northwestern Pacific generated by Typhoon Rammasun

in May 2008 using a moored ADCP. Observations of NIOs in this region have been rarely reported. The characteristics of anti-cyclonic eddy influence the propagation of NIOs. In general, NIOs propagate horizontally at the surface layer in the cyclonic eddy; on the other hand, they propagate vertically downward and are trapped in the anti-cyclonic eddy (Lee and Niller 1998). An anti-cyclonic eddy exists in mooring region when NIOs were generated by the typhoon and vertically propagated. The buoyancy frequency in the anti-cyclonic eddy varies due to the modification of water column structure, which can be also detected by the non-uniform characteristics of temperature and salinity in the eddy.

The typhoon-induced NIOs are trapped in depths of buoyancy frequency peaks during their downward propagation with a maximum ($= 18 \text{ J m}^{-3}$) at 210 m. The NIOs occurred by Rammasun transfer 71% of their total energy ($19.3 \times 10^{-2} \text{ W m}^{-2}$) into eddy core, and remain 29% in the upper layers. The concentrated NIO energy at the depths of 120 and 210 m persisted for about two weeks within the eddy. Vertical propagation speed of NIO energy becomes gradually faster with increasing depths and the frequency of NIOs increases gradually from $0.92f$ to $1.05f$ in the anti-cyclonic eddy. The increased vertical propagation speed is caused by the anti-cyclonic eddy existing near the mooring site during the period of the measurements. The change of NIO frequencies appears to be related to the relative vorticity in the anti-cyclonic eddy, which changes its magnitude from smaller to larger than local inertial frequency. The modification of the frequency of NIOs is identified when they interact with mesoscale eddies during their downward propagation in the open sea, which is similar to the previ-

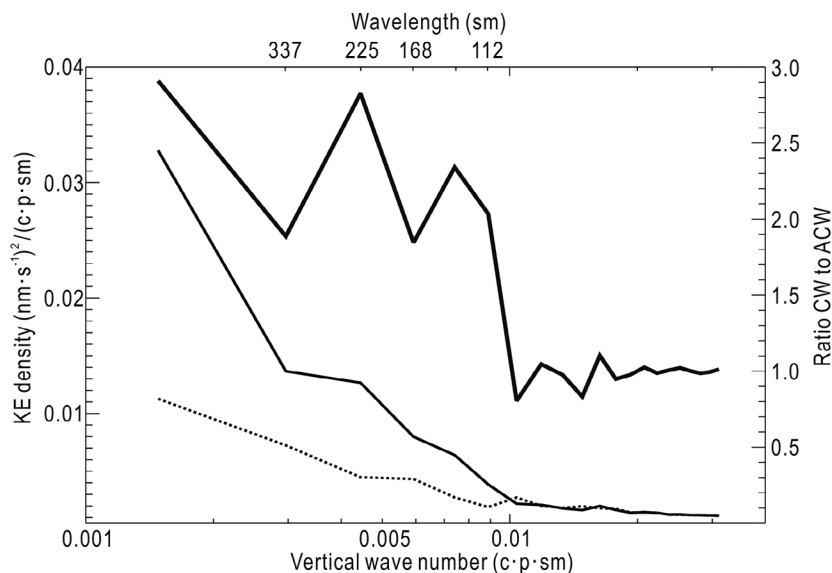


Fig. 9. Vertical rotary spectra of the WKB normalized velocity components between 3.5 and 5.5 IP (May 14, 03:00 ~ May 17, 18:00). Dotted curve is anti-clockwise component, thin curve is clockwise component, and thick one is the ratio of clockwise to anti-clockwise energies.

ous results measured by Morozov and Velarde (2008) and Jaimes and Shay (2010).

Kunze (1985) suggests that NIOs are trapped and amplified in the regions of negative vorticity such as anti-cyclonic eddies where the intrinsic frequency of NIO can be less than the effective Coriolis frequency. The ratio of effective to local Coriolis frequencies, the former of which is calculated from the data-assimilated HYCOM output, is smaller after the typhoon than before, and the depth where the effective Coriolis frequency is equivalent to the local frequency deepens from 200 to 280 m after the typhoon. Typhoon-induced NIOs are not scattered in the surface due to the change of effective Coriolis frequency by anti-cyclonic eddy, and propagate vertically downward and trapped in the eddy core. NIOs can penetrate down to 280 m where the ratio of effective to local Coriolis frequencies becomes one. They appear to lose their energy by turbulence at depths below 240 m as Kunze et al. (1995) suggested.

Our results in this study suggest that typhoon-induced NIOs interacting with meso-scale eddies can play an important role in providing the energy source available for ocean mixing in the tropical regions. Further studies using observations and numerical simulations are needed for better understanding of the associated physical processes.

Acknowledgements This work was supported by the POSEIDON (northwestern Pacific Ocean Study on Environment and Interactions between Deep Ocean and marginal seas) Project of Korea Institute of Ocean Science & Technology (PE99162).

REFERENCE

- Alford, M. H., 2003: Redistribution of energy available for ocean mixing by long-range propagation of internal waves. *Nature*, **423**, 159-162, doi: 10.1038/nature01628. [[Link](#)]
- Alford, M. H. and M. Whitmont, 2007: Seasonal and spatial variability of near-inertial kinetic energy from historical moored velocity records. *J. Phys. Oceanogr.*, **37**, 2022-2037, doi: 10.1175/JPO3106.1. [[Link](#)]
- Anderson, D. L. T. and A. E. Gill, 1979: Beta dispersion of inertial waves. *J. Geophys. Res.*, **84**, 1836-1842, doi: 10.1029/JC084iC04p01836. [[Link](#)]
- Byun, S.-S., J. J. Park, K.-I. Chang, and R. W. Schmitt, 2010: Observation of near-inertial wave reflections within the thermocline layer of an anticyclonic mesoscale eddy. *Geophys. Res. Lett.*, **37**, L01606, doi: 10.1029/2009GL041601. [[Link](#)]
- Dickey, T., D. Frye, J. McNeil, D. Manov, N. Nelson, D. Sigurdson, H. Jannasch, D. Siegel, T. Michaels, and R. Johnson, 1998: Upper-ocean temperature response to hurricane Felix as measured by the Bermuda testbed mooring. *Mon. Weather Rev.*, **126**, 1195-1201, doi: 10.1175/1520-0493(1998)126<1195:UOTRTH>2.0.CO;2. [[Link](#)]
- Dukhovskoy, D. S., S. L. Morey, and J. J. O'Brien, 2009: Generation of baroclinic topographic waves by a tropical cyclone impacting a low-latitude continental shelf. *Cont. Shelf Res.*, **29**, 333-351, doi: 10.1016/j.csr.2008.01.007. [[Link](#)]
- Gerkema, T. and V. I. Shrira, 2005: Near-inertial waves in the ocean: Beyond the 'traditional approximation'. *J. Fluid Mech.*, **529**, 195-219, doi: 10.1017/S0022112005003411. [[Link](#)]
- Jaimes, B. and L. K. Shay, 2010: Near-inertial wave wake of Hurricanes Katrina and Rita over mesoscale oceanic eddies. *J. Phys. Oceanogr.*, **40**, 1320-1337, doi: 10.1175/2010JPO4309.1. [[Link](#)]
- Kunze, E., 1985: Near-inertial wave propagation in geostrophic shear. *J. Phys. Oceanogr.*, **15**, 544-565, doi: 10.1175/1520-0485(1985)015<0544:NIWPIG>2.0.CO;2. [[Link](#)]
- Kunze, E. and T. B. Sanford, 1984: Observations of near-inertial waves in a front. *J. Phys. Oceanogr.*, **14**, 566-581, doi: 10.1175/1520-0485(1984)014<0566:OONIWI>2.0.CO;2. [[Link](#)]
- Kunze, E., R. W. Schmitt, and J. M. Toole, 1995: The energy balance in a warm-core ring's near-inertial critical layer. *J. Phys. Oceanogr.*, **25**, 942-957, doi: 10.1175/1520-0485(1995)025<0942:TEBIAW>2.0.CO;2. [[Link](#)]
- Leaman, K. D. and T. B. Sanford, 1975: Vertical energy propagation of inertial waves: A vector spectral analysis of velocity profiles. *J. Geophys. Res.*, **80**, 1975-1978, doi: 10.1029/JC080i015p01975. [[Link](#)]
- Lee, D.-K. and P. P. Niiler, 1998: The inertial chimney: The near-inertial energy drainage from the ocean surface to the deep layer. *J. Geophys. Res.*, **103**, 7579-7591, doi: 10.1029/97JC03200. [[Link](#)]
- Lueck, R. and T. Osborn, 1986: The dissipation of kinetic energy in a warm-core ring. *J. Geophys. Res.*, **91**, 803-818, doi: 10.1029/JC091iC01p00803. [[Link](#)]
- Morozov, E. G. and M. G. Velarde, 2008: Inertial oscillations as deep ocean response to hurricanes. *J. Oceanogr.*, **64**, 495-509, doi: 10.1007/s10872-008-0042-0. [[Link](#)]
- Park, J.-H. and D. R. Watts, 2005: Near-inertial oscillations interacting with mesoscale circulation in the southwestern Japan/East Sea. *Geophys. Res. Lett.*, **32**, L10611, doi: 10.1029/2005GL022936. [[Link](#)]
- Park, J.-H., K. A. Donohue, D. R. Watts, and L. Rainville, 2010: Distribution of deep near-inertial waves observed in the Kuroshio Extension. *J. Oceanogr.*, **66**, 709-717, doi: 10.1007/s10872-010-0058-0. [[Link](#)]
- Park, J. J., K. Kim, and R. W. Schmitt, 2009: Global distribution of the decay timescale of mixed layer inertial motions observed by satellite-tracked drifters. *J. Geo-*

- phys. Res.*, **114**, C11010, doi: 10.1029/2008JC005216. [[Link](#)]
- Price, J. F., 1983: Internal wave wake of a moving storm. Part I. Scales, energy budget and observations. *J. Phys. Oceanogr.*, **13**, 949-965, doi: 10.1175/1520-0485(1983)013<0949:IWWOAM>2.0.CO;2. [[Link](#)]
- Price, J. F., T. B. Sanford, and G. Z. Forristall, 1994: Forced stage response to a moving hurricane. *J. Phys. Oceanogr.*, **24**, 233-260, doi: 10.1175/1520-0485(1994)024<0233:FSRTAM>2.0.CO;2. [[Link](#)]
- Rossby, H. T. and T. B. Sanford, 1976: A study of velocity profiles through the main thermocline. *J. Phys. Oceanogr.*, **6**, 766-774, doi: 10.1175/1520-0485(1976)006<0766:ASOVPT>2.0.CO;2. [[Link](#)]
- Sliver, R. L. and M. Huber, 2007: Observational evidence for an ocean heat pump induced by tropical cyclones. *Nature*, **447**, 577-580, doi: 10.1038/nature05785. [[Link](#)]
- Wallcraft, A. J., E. J. Metzger, and S. N. Carroll, 2009: Software Design Description for the HYbrid Coordinate Ocean Model (HYCOM) Version 2.2, Naval Research Laboratory, NRL/MR/7320-09-9166, 149 pp.
- Zhai, X., R. J. Greatbatch, and J. Sheng, 2004: Advective spreading of storm-induced inertial oscillations in a model of the northwest Atlantic Ocean. *Geophys. Res. Lett.*, **31**, L14315, doi: 10.1029/2004GL020084. [[Link](#)]
- Zheng, Q., R. J. Lai, N. E. Huang, J. Pan, and W. T. Liu, 2006: Observation of ocean current response to 1998 Hurricane Georges in the Gulf of Mexico. *Acta Oceanol. Sin.*, **25**, 1-14.